

# Lattice Boltzmann Algorithm for three-dimensional liquid crystal hydrodynamics

C. Denniston<sup>1</sup>, D. Marenduzzo<sup>2</sup>, E. Orlandini<sup>3</sup>, and J.M. Yeomans<sup>2</sup>

<sup>1</sup>*Department of Applied Mathematics,*

*The University of Western Ontario, London, Ontario N6A 5B8, Canada*

<sup>2</sup>*Department of Physics, Theoretical Physics,*

*1 Keble Road, Oxford, OX1 3NP, England*

<sup>3</sup>*INFM, Dipartimento di Fisica, Universita' di Padova, Via Marzolo 8, 35131 Padova, Italy*

## Abstract

We describe a lattice Boltzmann algorithm to simulate liquid crystal hydrodynamics in three dimensions. The equations of motion are written in terms of a tensor order parameter. This allows both the isotropic and the nematic phases to be considered. Backflow effects and the hydrodynamics of topological defects are naturally included in the simulations, as are viscoelastic effects such as shear-thinning and shear-banding. We describe the implementation of velocity boundary conditions and show that the algorithm can be used to describe optical bounce in twisted nematic devices and secondary flow in sheared nematics with an imposed twist.

## I. INTRODUCTION

Liquid crystals are fluids, typically comprising long thin molecules. Subtle energy-entropy balances can cause the molecules to align to form a variety of ordered states. For example, in nematic liquid crystals, the molecules tend to align parallel giving a state with long-range orientational order. Liquid crystals exhibit both an elastic and a viscous response to an external stress. Coupling between the director and velocity fields leads to strongly non-Newtonian flow behaviour such as shear-banding and molecular tumbling under an applied shear.

Given both the rich rheological behaviour of liquid crystals and their importance in optical devices there is need to develop a robust numerical method to allow us to explore their dynamics. The hydrodynamic equations of motion are complex and, although much interesting analytic work has been carried out (see de Gennes & Prost 1993, Beris & Edwards 1994, and the recent review Rey & Denn 2002), there are many interesting questions that cannot be answered analytically. Therefore, in this paper, we describe a lattice Boltzmann approach to liquid crystal hydrodynamics in three dimensions. This generalizes a two dimensional algorithm which was proposed by Denniston et al. (2000). For a review of the lattice Boltzmann algorithm see Chen & Doolen (1998), S. Succi (2000), Wolf-Gladrow (2000), R. Benzi et al. (1992).

We first summarize the Beris-Edwards equations of motion for nematic liquid crystals (Beris *et al.*, 1990,1994). The lattice Boltzmann algorithm is described in some detail. We pay specific attention to boundary conditions which can be more cumbersome in three dimensions than in two. We then present two examples, switching in a twisted nematic device and shear flow in a twisted nematic, to illustrate the applicability of the method.

## II. MODELLING LIQUID CRYSTAL HYDRODYNAMICS

### A. Equations of motion

Liquid crystals are described in terms of a local tensor order parameter  $\mathbf{Q}$ , that is related to the direction of individual molecules  $\hat{m}$  by  $Q_{\alpha\beta} = \langle \hat{m}_\alpha \hat{m}_\beta - \frac{1}{3} \delta_{\alpha\beta} \rangle$ , where the angular brackets denote a coarse-grained average. Greek indices will be used to represent Cartesian components of vectors and tensors, and the usual summation over repeated indices will be assumed.  $\mathbf{Q}$  is a traceless symmetric tensor. Its largest eigenvalue,  $\frac{2}{3}q$ ,  $0 < q < 1$ , describes the magnitude of order along its principle eigenvector  $\hat{n}$ , referred to as the director.

The order parameter evolves according to the equation (Beris *et al.*, 1990,1994)

$$(\partial_t + \vec{u} \cdot \nabla) \mathbf{Q} - \mathbf{S}(\mathbf{W}, \mathbf{Q}) = \Gamma \mathbf{H} \quad (\text{II.1})$$

where  $\Gamma$  is a collective rotational diffusion constant and

$$\begin{aligned} \mathbf{S}(\mathbf{W}, \mathbf{Q}) = & (\xi \mathbf{D} + \mathbf{\Omega})(\mathbf{Q} + \mathbf{I}/3) + (\mathbf{Q} + \mathbf{I}/3)(\xi \mathbf{D} - \mathbf{\Omega}) \\ & - 2\xi(\mathbf{Q} + \mathbf{I}/3)\text{Tr}(\mathbf{Q}\mathbf{W}) \end{aligned} \quad (\text{II.2})$$

where  $\mathbf{D} = (\mathbf{W} + \mathbf{W}^T)/2$  and  $\mathbf{\Omega} = (\mathbf{W} - \mathbf{W}^T)/2$  are the symmetric part and the anti-symmetric part respectively of the velocity gradient tensor  $W_{\alpha\beta} = \partial_\beta u_\alpha$ . The mixture of upper and lower convective derivatives is governed by the constant  $\xi$ , which depends on the molecular details of a given liquid crystal.

The term on the right-hand side of Eq.(II.1) describes the relaxation of the order parameter towards the minimum of the free energy. The driving motion is provided by the molecular field  $\mathbf{H}$ , which is related to the variational derivative of the free energy  $\mathcal{F}$  by

$$\mathbf{H} = -\frac{\delta \mathcal{F}}{\delta \mathbf{Q}} + (\mathbf{I}/3)\text{Tr} \frac{\delta \mathcal{F}}{\delta \mathbf{Q}} \quad (\text{II.3})$$

The symmetry and zero trace of  $\mathbf{Q}$  (and  $\mathbf{H}$ ) is exploited for simplification.

The fluid has density  $\rho$  and obeys both the continuity equation

$$\partial_t \rho + \partial_\alpha \rho u_\alpha = 0 \quad (\text{II.4})$$

and the Navier-Stokes equation

$$\rho \partial_t u_\alpha + \rho u_\beta \partial_\beta u_\alpha = \partial_\beta \tau_{\alpha\beta} + \partial_\beta \sigma_{\alpha\beta} + \frac{\rho \tau_f}{3} (\partial_\beta ((\delta_{\alpha\beta} - 3\partial_\rho P_0) \partial_\gamma u_\gamma + \partial_\alpha u_\beta + \partial_\beta u_\alpha)). \quad (\text{II.5})$$

The form of this equation is similar to that for a simple fluid. However, the details of the stress tensor reflect the additional complications of liquid crystal hydrodynamics. There is a symmetric contribution

$$\begin{aligned} \sigma_{\alpha\beta}^E = & -P_0 \delta_{\alpha\beta} - \xi H_{\alpha\gamma} (Q_{\gamma\beta} + \frac{1}{3} \delta_{\gamma\beta}) - \xi (Q_{\alpha\gamma} + \frac{1}{3} \delta_{\alpha\gamma}) H_{\gamma\beta} \\ & + 2\xi (Q_{\alpha\beta} + \frac{1}{3} \delta_{\alpha\beta}) Q_{\gamma\epsilon} H_{\gamma\epsilon} - \partial_\beta Q_{\gamma\nu} \frac{\delta \mathcal{F}}{\delta \partial_\alpha Q_{\gamma\nu}} \end{aligned} \quad (\text{II.6})$$

and an antisymmetric contribution

$$\tau_{\alpha\beta} = Q_{\alpha\gamma} H_{\gamma\beta} - H_{\alpha\gamma} Q_{\gamma\beta}. \quad (\text{II.7})$$

The hydrostatic pressure  $P_0$  is defined below, while  $\eta \equiv \frac{\rho\tau_f}{3}$  is an isotropic viscosity ( $\tau_f$  is related to the details of the lattice Boltzmann algorithm, see Eq. II.16). If more elastic constants are introduced in the theory,  $\tau_{\alpha\beta}$  also contains the antisymmetric contribution from  $\partial_\beta Q_{\gamma\nu} \frac{\delta\mathcal{F}}{\delta\partial_\alpha Q_{\gamma\nu}}$ .

The lattice Boltzmann algorithm described in the next subsection can be used for any model of the above form. For the examples in the last section we will use a specific model determined by a Landau-de Gennes free energy (de Gennes & Prost, 1993; Doi & Edwards, 1989)

$$\mathcal{F} = \int d^3r \left\{ \frac{A_0}{2} \left(1 - \frac{\gamma}{3}\right) Q_{\alpha\beta}^2 - \frac{A_0\gamma}{3} Q_{\alpha\beta} Q_{\beta\gamma} Q_{\gamma\alpha} + \frac{A_0\gamma}{4} (Q_{\alpha\beta}^2)^2 + \frac{\kappa}{2} (\partial_\alpha Q_{\beta\lambda})^2 \right\} \quad (\text{II.8})$$

where  $A_0$  is a constant and  $\kappa$  denotes the elastic constant of the liquid crystal. We shall work within the one elastic constant approximation. Although it is not hard to include more general elastic terms this simplification will not affect the qualitative behaviour. The free energy (II.8) describes a first order transition from the isotropic to the nematic phase, controlled by the parameter  $\gamma$ . The hydrostatic pressure  $P_0$  is taken to be

$$P_0 = \rho T - \frac{\kappa}{2} (\nabla \mathbf{Q})^2, \quad (\text{II.9})$$

and is constant in the simulations to a very good approximation.

## B. Lattice Boltzmann algorithm

Usually lattice Boltzmann algorithms, describing the Navier-Stokes equations of a simple fluid, are defined in terms of a single set of partial distribution functions, the scalars  $f_i(\vec{x})$ , that sum on each lattice site  $\vec{x}$  to give the density (Chen & Doolen 1998). For liquid crystal hydrodynamics, this must be supplemented by a second set, the symmetric traceless tensors  $\mathbf{G}_i(\vec{x})$ , that are related to the tensor order parameter  $\mathbf{Q}$ . Each  $f_i$ ,  $\mathbf{G}_i$  is associated with a lattice vector  $\vec{e}_i$ . We choose a 15-velocity model on the cubic lattice with lattice vectors:

$$\vec{e}_i^{(0)} = (0, 0, 0) \quad (\text{II.10})$$

$$\vec{e}_i^{(1)} = (\pm 1, 0, 0), (0, \pm 1, 0), (0, 0, \pm 1) \quad (\text{II.11})$$

$$\vec{e}_i^{(2)} = (\pm 1, \pm 1, \pm 1). \quad (\text{II.12})$$

The indices,  $i$ , are ordered so that  $i = 0$  corresponds to  $\vec{e}_i^{(0)}$ ,  $i = 1, \dots, 6$  correspond to the  $\vec{e}_i^{(1)}$  set and  $i = 7, 14$  to the  $\vec{e}_i^{(2)}$  set, as illustrated in Fig. 1.

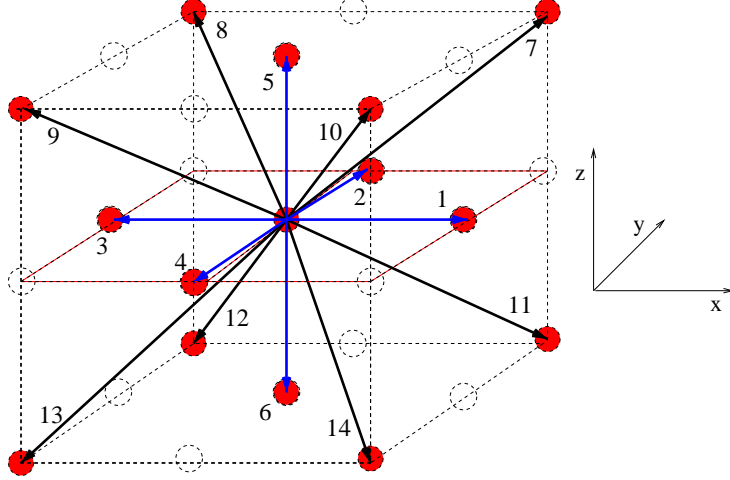


FIG. 1: Lattice geometry and lattice vectors for the three dimensional lattice Boltzmann model.

Physical variables are defined as moments of the distribution function:

$$\rho = \sum_i f_i, \quad \rho u_\alpha = \sum_i f_i e_{i\alpha}, \quad \mathbf{Q} = \sum_i \mathbf{G}_i. \quad (\text{II.13})$$

The distribution functions evolve in a time step  $\Delta t$  according to

$$f_i(\vec{x} + \vec{e}_i \Delta t, t + \Delta t) - f_i(\vec{x}, t) = \frac{\Delta t}{2} [\mathcal{C}_{f_i}(\vec{x}, t, \{f_i\}) + \mathcal{C}_{f_i}(\vec{x} + \vec{e}_i \Delta t, t + \Delta t, \{f_i^*\})] \quad (\text{II.14})$$

$$\mathbf{G}_i(\vec{x} + \vec{e}_i \Delta t, t + \Delta t) - \mathbf{G}_i(\vec{x}, t) = \frac{\Delta t}{2} [\mathcal{C}_{\mathbf{G}_i}(\vec{x}, t, \{\mathbf{G}_i\}) + \mathcal{C}_{\mathbf{G}_i}(\vec{x} + \vec{e}_i \Delta t, t + \Delta t, \{\mathbf{G}_i^*\})] \quad (\text{II.15})$$

This represents free streaming with velocity  $\vec{e}_i$  followed by a collision step which allows the distribution to relax towards equilibrium.  $f_i^*$  and  $\mathbf{G}_i^*$  are first order approximations to  $f_i(\vec{x} + \vec{e}_i \Delta t, t + \Delta t)$  and  $\mathbf{G}_i(\vec{x} + \vec{e}_i \Delta t, t + \Delta t)$  respectively. They are obtained by using  $\Delta t \mathcal{C}_{f_i}(\vec{x}, t, \{f_i\})$  on the right hand side of Eq. (II.14) and a similar substitution in Eq. (II.15). Discretizing in this way, which is similar to a predictor-corrector scheme, has the advantages that lattice viscosity terms are eliminated to second order and that the stability of the scheme is improved.

The collision operators are taken to have the form of a single relaxation time Boltzmann equation, together with a forcing term

$$\mathcal{C}_{f_i}(\vec{x}, t, \{f_i\}) = -\frac{1}{\tau_f} (f_i(\vec{x}, t) - f_i^{eq}(\vec{x}, t, \{f_i\})) + p_i(\vec{x}, t, \{f_i\}), \quad (\text{II.16})$$

$$\mathcal{C}_{\mathbf{G}_i}(\vec{x}, t, \{\mathbf{G}_i\}) = -\frac{1}{\tau_G} (\mathbf{G}_i(\vec{x}, t) - \mathbf{G}_i^{eq}(\vec{x}, t, \{\mathbf{G}_i\})) + \mathbf{M}_i(\vec{x}, t, \{\mathbf{G}_i\}). \quad (\text{II.17})$$

The form of the equations of motion and thermodynamic equilibrium follow from the choice of the moments of the equilibrium distributions  $f_i^{eq}$  and  $\mathbf{G}_i^{eq}$  and the driving terms  $p_i$  and  $\mathbf{M}_i$ .  $f_i^{eq}$

is constrained by

$$\sum_i f_i^{eq} = \rho, \quad \sum_i f_i^{eq} e_{i\alpha} = \rho u_\alpha, \quad \sum_i f_i^{eq} e_{i\alpha} e_{i\beta} = -\sigma_{\alpha\beta} + \rho u_\alpha u_\beta \quad (\text{II.18})$$

where the zeroth and first moments are chosen to impose conservation of mass and momentum. The second moment of  $f^{eq}$  controls the symmetric part of the stress tensor, whereas the moments of  $p_i$

$$\sum_i p_i = 0, \quad \sum_i p_i e_{i\alpha} = \partial_\beta \tau_{\alpha\beta}, \quad \sum_i p_i e_{i\alpha} e_{i\beta} = 0 \quad (\text{II.19})$$

impose the antisymmetric part of the stress tensor. For the equilibrium of the order parameter distribution we choose

$$\sum_i \mathbf{G}_i^{eq} = \mathbf{Q}, \quad \sum_i \mathbf{G}_i^{eq} e_{i\alpha} = \mathbf{Q} u_\alpha, \quad \sum_i \mathbf{G}_i^{eq} e_{i\alpha} e_{i\beta} = \mathbf{Q} u_\alpha u_\beta. \quad (\text{II.20})$$

This ensures that the order parameter is convected with the flow. Finally the evolution of the order parameter is most conveniently modeled by choosing

$$\sum_i \mathbf{M}_i = \Gamma \mathbf{H}(\mathbf{Q}) + \mathbf{S}(\mathbf{W}, \mathbf{Q}) \equiv \hat{\mathbf{H}}, \quad \sum_i \mathbf{M}_i e_{i\alpha} = \left( \sum_i \mathbf{M}_i \right) u_\alpha \quad (\text{II.21})$$

which ensures that the fluid minimises its free energy at equilibrium. Conditions (II.18)–(II.21) are satisfied, as is usual in lattice Boltzmann schemes, by writing the equilibrium distribution functions and forcing terms as polynomial expansions in the velocity

$$\begin{aligned} f_i^{eq} &= A_s + B_s u_\alpha e_{i\alpha} + C_s u^2 + D_s u_\alpha u_\beta e_{i\alpha} e_{i\beta} + E_{s\alpha\beta} e_{i\alpha} e_{i\beta}, \\ \mathbf{G}_i^{eq} &= \mathbf{J}_s + \mathbf{K}_s u_\alpha e_{i\alpha} + \mathbf{L}_s u^2 + \mathbf{N}_s u_\alpha u_\beta e_{i\alpha} e_{i\beta}, \\ p_i &= T_s \partial_\beta \tau_{\alpha\beta} e_{i\alpha}, \\ \mathbf{M}_i &= \mathbf{R}_s + \mathbf{S}_s u_\alpha e_{i\alpha}, \end{aligned} \quad (\text{II.22})$$

where  $s \in \{0, 1, 2\}$  identifies separate coefficients for the velocity vectors  $\hat{e}_i^{(s)}$ . The coefficients are determined by evaluating the constraints Eqs. (II.18)–(II.21) and matching terms. In doing this, we have made use of the following symmetry relations for the lattice vectors, Eq.(II.12),

$$\sum_{i=1}^6 e_{i\alpha}^{(1)} = \sum_{i=7}^{14} e_{i\alpha}^{(2)} = 0 \quad \alpha = 1, 2, 3 \quad (\text{II.23})$$

$$\sum_{i=1}^6 e_{i\alpha}^{(1)} e_{i\beta}^{(1)} = 2\delta_{\alpha\beta} \quad \sum_{i=7}^{14} e_{i\alpha}^{(2)} e_{i\beta}^{(2)} = 8\delta_{\alpha\beta} \quad (\text{II.24})$$

$$\sum_{i=1}^6 e_{i\alpha}^{(1)} e_{i\beta}^{(1)} e_{i\eta}^{(1)} = \sum_{i=7}^{14} e_{i\alpha}^{(2)} e_{i\beta}^{(2)} e_{i\eta}^{(2)} = 0 \quad (\text{II.25})$$

$$\sum_{i=1}^6 e_{i\alpha}^{(1)} e_{i\beta}^{(1)} e_{i\eta}^{(1)} e_{i\zeta}^{(1)} = 2\delta_{\alpha\beta}\delta_{\beta\eta}\delta_{\eta\zeta} \quad (\text{II.26})$$

$$\sum_{i=7}^{14} e_{i\alpha}^{(2)} e_{i\beta}^{(2)} e_{i\eta}^{(2)} e_{i\zeta}^{(2)} = 8\Delta_{\alpha\beta\eta\zeta} - 16\delta_{\alpha\beta}\delta_{\beta\eta}\delta_{\eta\zeta}. \quad (\text{II.27})$$

where  $\Delta_{\alpha\beta\eta\zeta} = \delta_{\alpha\beta}\delta_{\eta\zeta} + \delta_{\alpha\eta}\delta_{\beta\zeta} + \delta_{\alpha\zeta}\delta_{\beta\eta}$ .

The expansion coefficients are then determined to be:

$$\begin{aligned} A_2 &= \frac{1}{10}(\text{Tr}\mathbf{P}/3), & A_1 &= A_2, & A_0 &= \rho - 14A_2, \\ B_2 &= \rho/24, & B_1 &= 8B_2, \\ C_2 &= -\frac{\rho}{24}, & C_1 &= 2C_2, & C_0 &= -\frac{2}{3}\rho, \\ D_2 &= \frac{\rho}{16}, & D_1 &= 8D_2 \\ E_{2\alpha\beta} &= \frac{1}{16}(-\sigma_{\alpha\beta} - \text{Tr}\mathbf{P}/3\delta_{\alpha\beta}), & E_{1\alpha\beta} &= 8E_{2\alpha\beta}, \\ \mathbf{J}_0 &= \mathbf{Q}, & \mathbf{K}_2 &= \mathbf{Q}/24, & \mathbf{K}_1 &= 8\mathbf{K}_2, \\ \mathbf{L}_2 &= -\frac{\mathbf{Q}}{24}, & \mathbf{L}_1 &= 2\mathbf{L}_2, & \mathbf{L}_0 &= -\frac{2\mathbf{Q}}{3}, \\ \mathbf{N}_2 &= \frac{\mathbf{Q}}{16}, & \mathbf{N}_1 &= 8\mathbf{N}_2 \\ \mathbf{R}_2 &= \widehat{\mathbf{H}}/15, & \mathbf{R}_1 &= \mathbf{R}_0 = \mathbf{R}_2 \\ \mathbf{S}_2 &= \frac{\widehat{\mathbf{H}}}{24}, & \mathbf{S}_1 &= 8\mathbf{S}_2, \\ T_2 &= 1/24, & T_1 &= 8T_2. \end{aligned} \quad (\text{II.28})$$

### C. Velocity boundary conditions

To illustrate the implementation of the boundary conditions for a system sheared along  $y$  consider a wall at  $z = 0$ . No flux across the wall at  $z = 0$  implies  $\sum_i f_i e_{iz} = 0$  and hence

$$f_5 + f_7 + f_8 + f_9 + f_{10} = f_6 + f_{11} + f_{12} + f_{13} + f_{14}. \quad (\text{II.29})$$

For no slip along the  $x$ -direction  $\sum_i f_i e_{ix} = 0$  or

$$f_1 + f_7 + f_{10} + f_{11} + f_{14} = f_3 + f_8 + f_9 + f_{12} + f_{13}. \quad (\text{II.30})$$

For fixed velocity  $u_y^*$  along the  $y$  direction  $\sum_i f_i e_{iy} = \rho u_y^*$  or

$$f_2 + f_7 + f_8 + f_{11} + f_{12} - f_4 - f_9 - f_{10} - f_{13} - f_{14} = \rho u_y^*. \quad (\text{II.31})$$

For the wall at  $z = 0$  there are 5 unknown distributions  $f_5, f_7, f_8, f_9$  and  $f_{10}$ . To determine these, two further constraints are required in addition to the relations (II.29), (II.30), and (II.31). Symmetry suggests

$$f_7 - f_8 = f_{10} - f_9. \quad (\text{II.32})$$

The conservation of mass is easily obtained by choosing

$$f_5 = f_6. \quad (\text{II.33})$$

Other choices can be made for these two further constraints. With the present one, equations (II.29)-(II.33) can now be solved to give:

$$\begin{aligned} f_5 &= f_6, \\ f_7 &= \frac{1}{4} \left( -f_1 - f_2 + f_3 + f_4 - f_{11} + f_{12} + 3f_{13} + f_{14} + \rho u_y^* \right), \\ f_8 &= \frac{1}{4} \left( f_1 - f_2 - f_3 + f_4 + f_{11} - f_{12} + f_{13} + 3f_{14} + \rho u_y^* \right), \\ f_9 &= \frac{1}{4} \left( f_1 + f_2 - f_3 - f_4 + 3f_{11} + f_{12} - f_{13} + f_{14} - \rho u_y^* \right), \\ f_{10} &= \frac{1}{4} \left( -f_1 + f_2 + f_3 - f_4 + f_{11} + 3f_{12} + f_{13} - f_{14} - \rho u_y^* \right). \end{aligned} \quad (\text{II.34})$$

### III. NUMERICAL RESULTS

Our main purpose here is to present in detail a numerical algorithm for simulating liquid crystal hydrodynamics in three dimensions. Consequently, we restrict ourselves to presenting a few simple examples, aimed at checking the approach. Further numerical applications are listed in the concluding section and will be reported elsewhere.

To apply the algorithm to systems of practical relevance, we need to map the simulation parameters listed in Section (2b) onto physical numbers which can be compared to real experiments. This task is not trivial and proceeds as follows. First, we have to fix a physical value for the energy scale, which in simulations is given by  $\rho T$ . Second, the size of the simulation lattice along  $z$ ,  $L_z$ , is matched to the liquid crystal cell thickness. Third, the parameter  $\Gamma$  is related to the magnitude of order and the physical value of the Miesowicz viscosity  $\gamma_1$  (see De Gennes & Prost 1993) via the formula  $\Gamma = 2q^2/\gamma_1$  (Denniston et al. 2001). This fixes the time step in the simulation. Once the energy, length and time scales are specified, all simulation parameters can be related straightforwardly to experimental quantities.



As specific examples of applications of the three-dimensional algorithm we propose two hydrodynamic effects in two commonly used twisted nematic cells. The simplest example of such cells is obtained when at the two surfaces (perpendicular to the  $z$ -axis, say) the director is anchored and the anchoring is homogeneous, i.e. the directors lie in the surface plane. If the two anchoring directions at  $z = 0$  and  $z = L_z$  are mutually perpendicular, the free energy minimum in the absence of other factors is a twisted director field along the  $z$  direction. This is the geometry we consider (with the two pinning directions making an angle of  $\pm\pi/4$  with the  $x$  axis to maximise the system symmetry).

In devices, this cell is switched on by means of an electric field perpendicular to the surfaces. Here we shall study the dynamics when the cell is switched off and relaxes back to the twisted state. Therefore we initialize the director field to lie along the  $z$  direction in the whole cell apart from two small regions (8 lattice sites in our simulations) near the top and bottom boundaries to allow a smooth relaxation between surface and bulk order. The numerical parameters used for this calculation were as follows:  $\kappa = 0.05$ ,  $\gamma = 3.5$ ,  $L_z = 91$ ,  $\Gamma = 0.33775$ ,  $\xi = 0.8$  and  $\tau_f = 0.56$ . By means of the procedure outlined above, the simulation system can be mapped onto a physical device of thickness  $4.5 \mu m$ , with all three Frank elastic constants equal to  $\sim 9.3$  pN, while  $\Gamma = 0.58$  Poise $^{-1}$  and the Miesowicz coefficient  $\gamma_1 = 1.3$  Poise.

In Fig. 2 we show how the tilt,  $\theta$ , of the director in the midplane ( $z = L_z/2$ ) changes as a function of time immediately after the device is switched off. (The tilt angle is the angle with respect to the  $xy$  plane). In the figure we compare the results obtained when backflow is neglected and when it is included. It can be seen that backflow has a significant effect on the switching, namely it causes the non-monotonicity in the relaxation dynamics of the mid-plane tilt angle. The flow in the device causes the director to start its relaxation in the 'wrong' direction. As the system is symmetric the mid-plane tilt has to pass through  $90^\circ$  again during the relaxation to the twisted state. This is a known effect which is called of optical bounce. Note also that with backflow the relaxation is faster.

Optical bounce has only recently been observed directly in an experiment (Smith et al. 2002, Ruan et al. 2002). Our curve compares qualitatively well with the one observed by Ruan et al., who use a cell of comparable thickness and  $\gamma_1$  value, but with a slightly larger value of the elastic constants. In the experiments, the maximum in the tilt angle occurred for a value of  $\theta \sim 96^\circ$ , the backflow effect lasted  $\sim 2$  ms, and after 10 ms the angle had relaxed down to  $\sim 60^\circ$ . Since the details of the dynamics depend on the width of the region which is initially oriented along  $z$  and

on the temperature, we are satisfied with semiquantitative agreement here.

The optical bounce can be seen within Leslie-Ericksen theory (see e.g. Kelly et al. 1999). However with the Beris-Edwards equations solved here we can also investigate the dependence of the dynamics on temperature. The bounce gets deeper as the effective temperature is decreased for constant  $\kappa$ , or if  $\kappa$  is increased at constant  $\gamma$ . Interestingly, as the temperature increases and approaches the isotropic-to-nematic transition point, the waiting time needed for the system to start the bounce increases. This happens because the magnitude of the order near the surface, where the initial director deformations are confined, drops significantly allowing two defects to transiently form. These defects block the system evolution and slow down the start-up of the dynamics. Furthermore, we can assess the effect of tuning the strength of anchoring and the magnitude of surface order on the bounce magnitude: while the former has a negligible effect on the result, the latter can have a bigger impact, i.e. if the order within the surface is slightly different from the typical order within the bulk, the bounce magnitude can change significantly.

As a second example, we consider another twisted geometry, in which the director is anchored parallel on the two boundaries, and a  $\pi$  twist is introduced in the  $z$  direction. We consider a shear experiment in which the bounding plates move at constant velocities  $\pm u_y$ . Because the director does not lie in the shear plane, (the  $yz$  plane), the hydrodynamics is complex. In particular, experiments and approximate modelling (using the Leslie-Ericksen equations) predict that even though the system is sheared along  $y$ , a secondary flow appears along the  $x$  direction (De Gennes & Prost 1993).

In Figure 3, we show that the lattice Boltzmann simulations can reproduce this three-dimensional feature well. In the same figure, we also show how the director field components  $n_x$ ,  $n_y$  and  $n_z$  vary across the cell. These results were obtained for simulation parameters  $\kappa = 0.05$ ,  $\gamma = 3.5$ ,  $L_z = 51$ ,  $\Gamma = 0.33775$ ,  $\xi = 0.85$  and  $\tau_f = 0.56$ , which can be mapped this time onto a physical device of thickness  $2.25 \mu m$ , with all three Frank elastic constants equal to  $\sim 3.3$  pN.

#### IV. DISCUSSION

In this paper we have described in detail a lattice Boltzmann algorithm to simulate liquid crystal hydrodynamics in three dimensions. We have shown that it can, for values of the simulation parameters which capture physical nematic properties and device dimensions, reproduce optical bounce in a twisted nematic device and secondary flow in a twisted nematic under shear. Future

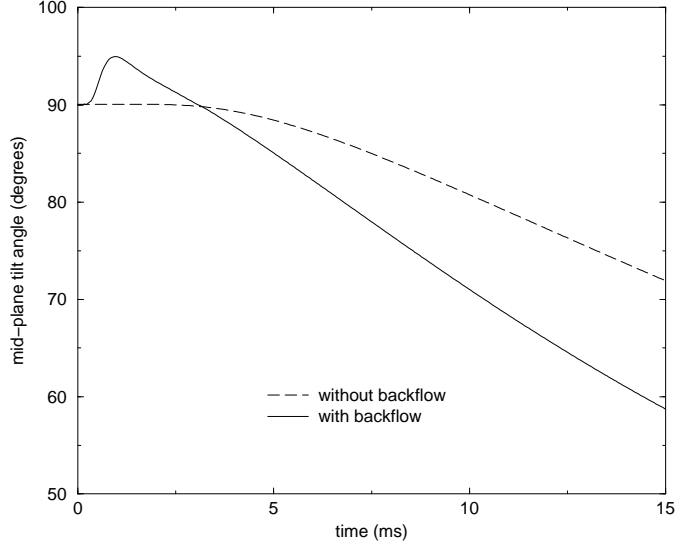


FIG. 2: Evolution of the tilt of the director field at the centre of a twisted nematic cell after the field is switched off. Notice that  $\theta$  and  $\pi - \theta$  actually represent the same state since the director field has no 'head' or 'tail'.

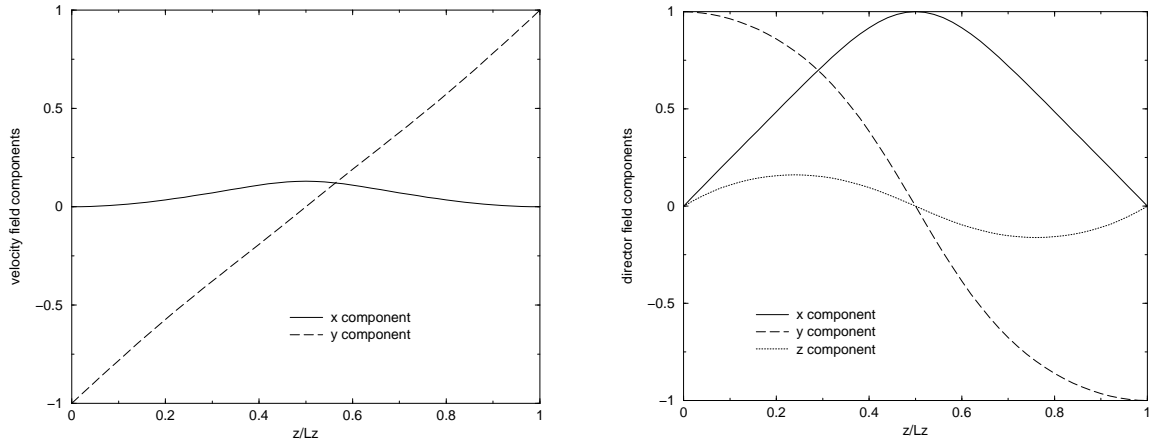


FIG. 3: Velocity field (left) and director field (right) as a function of the position across the cell for a  $\pi$  twisted nematic liquid crystal under shear. Note the secondary flow along  $x$  in the left figure. The velocity profile in the left plot is scaled by the shearing velocity, which was  $\sim 0.8$  mm/s.

applications will include studying backflow in more complicated device geometries such a pi-cell (Jung et al. 2003) and 4-domain twisted nematic cells. It will also be of interest to consider the flow of liquid crystals in narrow channels as, with the advent of microchannel technology, quantitative experiments may soon become possible. Here, surface anchoring and elastic deformations of the director field are expected to heavily impact on the rheological properties (Marenduzzo et al. 2003). Other areas where this approach will be useful is in the study of shear banding under

both constant stress and constant strain and in considering the flow of cholesterics, nematic liquid crystals with a director field that form a helix.

- 
- [0] P.G. de Gennes & J. Prost 1993, *The Physics of Liquid Crystals, 2nd Ed.*, Clarendon Press, Oxford, (1993).
- [0] A.N. Beris & B.J. Edwards 1994, *Thermodynamics of Flowing Systems*, Oxford: Oxford University Press.
- [0] A. D. Rey & M. M. Denn 2002, Dynamical phenomena in liquid-crystalline materials, *Annu. Rev. Fluid Mech.* **34**, 233-266.
- [0] A.N. Beris, B.J. Edwards & M. Grmela 1990, Generalized constitutive equation for polymeric liquid-crystals. 1. Model formulation using the Hamiltonian (Poisson bracket) formulation *J. Non-Newton. Fluid Mechanics*, **35** 51-72.
- [0] S. Chen & G. D. Doolen 1998, Lattice Boltzmann method for fluid flows, *Annu. Rev. Fluid Mech.* **30**, 329-364.
- [0] S. Succi 2001, *The lattice Boltzmann equation for fluid dynamics and beyond*, Oxford University Press.
- [0] D. A. Wolf-Gladrow 2000, *Lattice-gas cellular automata and lattice Boltzmann models*, Vol. 1725, Springer, Berlin.
- [0] R. Benzi, S. Succi, M. Vergassola 1992, The lattice Boltzmann equation: theory and applications, *Phys. Rep.* **222**, 145-197.
- [0] M. Doi & S. F. Edwards 1989, *The Theory of Polymer Dynamics*, Clarendon Press, Oxford.
- [0] C. Denniston, E. Orlandini & J. M. Yeomans 2000, Simulations of liquid crystal hydrodynamics in the isotropic and nematic phases, *Europhys. Lett.* **52**, 481-487.
- [0] C. Denniston, E. Orlandini & J. M. Yeomans 2001, Lattice Boltzmann simulations of liquid crystal hydrodynamics, *Phys. Rev. E* **63**, 056702.
- [0] N. J. Smith, M. D. Tillin & J. R. Sambles 2002, Direct optical quantification of backflow in a 90 degrees twisted nematic cell, *Phys. Rev. Lett.* **88**, 088301.
- [0] L. Z. Ruan & J. R. Sambles 2002, Dynamics of a twisted nematic cell using a convergent beam system, *J. Appl. Phys.* **92**, 4857-4862.
- [0] J. Kelly, S. Jamal & M. Cui 1999, Simulation of the dynamics of twisted nematic devices including flow, *J. Appl. Phys.* **86**, 4091-4095.
- [0] J. Jung, C. Denniston, E. Orlandini & J. M. Yeomans 2003, Anisotropy of domain growth in nematic liquid crystals, *Liquid Crystals* in press.
- [0] D. Marenduzzo, E. Orlandini & J. M. Yeomans 2003, Rheology of distorted nematic liquid crystals, *Europhys. Lett.*, **64**, 406-412.